J. Fluid Mech. (1991), *vol.* 232, *pp.* 591–609
Printed in Great Britain

Structure and mechanism of oscillatory convection in a cube of fluid-saturated porous material heated from below

By MICHAEL D. GRAHAM AND PAUL H. STEEN
School of Chemical Engineering, Cornell University, Ithaca, NY 14853, USA

(Received 29 January 1990 and in revised form 29 March 1991)

The transition from steady to oscillatory three-dimensional convection in a cube of saturated porous material is calculated to occur at Rayleigh number $R = 584$ due to seven pairs of thermal blobs which circulate around the cube. This travelling wave instability is shown to be closely related, first as regards structural characteristics and then as regards mechanism of instability, to an analogous instability in two dimensions. The correspondence with the two-dimensional flow is established via a correspondence with a nonlinear base flow in a box of square planform of a different aspect ratio $(1/\sqrt{2})$ and ultimately derives from the symmetries of the base flow in the cube.

1. Introduction

Viscous fluid in a saturated porous material can be unstable to buoyancy-driven convection. In a closed container convection undergoes a sequence of transitions as the temperature difference from bottom to top is increased, much like those observed in the Rayleigh–Bénard system. In a cubic box, the transition to time-dependence occurs as an oscillatory three-dimensional motion that replaces the steady three-dimensional pattern. The main result reported here is that the spatial structure of the destabilizing flow can be characterized as a rather simple travelling wave. Indeed, the Rayleigh number of the transition and the number of thermal cells (or vortical cells) in the destabilizing disturbance can be explained as a modification of what occurs for the two-dimensional layer with finite sidewalls, where the wave travels in a loop with a speed typical of the base-state motion and with a structure that balances self-induced convection with thermal diffusion. This is consistent with the observations of Kimura, Schubert & Straus (1989) that the sequences of transitions in two- and three-dimensional porous media are analogous.

Recent numerical simulations of the Rayleigh–Bénard system are mostly large-scale computations (which typically solve initial-value problems) ostensibly aimed at capturing as many flow details as possible as far into the nonlinear regime as possible. In contrast are the attempts to interpret observations (experiment and simulation) from a dynamical systems point of view. Here there has been some success in identifying various routes to chaos, which typically include period-doubling, quasi-periodic and intermittent behaviour. However, the emphasis remains on temporal behaviour, and descriptions of spatial structures and their interactions with the dynamics are generally lacking. We show below that for the porous media analogue of the Rayleigh–Bénard system the transition to time-dependence is accurately

described by a simple physical picture. Moreover, this picture necessarily couples the spatial and temporal behaviour.

Experiments associated with fluid-saturated porous media are more difficult than those with pure fluids owing to the presence of the solid phase. On the other hand, the well-accepted model (i.e. governing equations) for the porous media system has several distinct advantages over its counterpart in the Rayleigh–Bénard problem. The porous media equations on three-dimensional domains have been proved to have strong solutions globally in time (Fabrie 1986). This leads to the existence of a global attractor, estimates of its size and, in general, places the dynamical systems approach to this problem on a firm mathematical foundation (Titi 1991). Analogous results for the three-dimensional pure fluid case have not been forthcoming (nor have they in the case of the three-dimensional Navier–Stokes equations). There are also advantages to the porous media model from the point of view of computations. The governing equations, with realistic boundary conditions, admit a complete set of simple basis functions generated by a linear self-adjoint operator; this makes the problem especially suited to solution by spectral or pseudo-spectral techniques.

Several authors (Horne 1979; Kimura *et al.* 1989; Stamps, Arpaci & Clark 1990) include the transition to time-dependence in their studies of three-dimensional porous media convection in a cube. Kimura *et al.* (1989, hereinafter referred to as KSS) have some of the most complete results. They solve an initial-value problem many times over using the pseudo-spectral approach in order to construct a sequence of transitions which lead from steady motion S, to a steady 'less symmetric' motion S′, to time-periodic P′, quasi-periodic QP, and back to a periodic motion P^2 for Rayleigh numbers ranging from convection onset ($R_c = 4.5\pi^2$) to sixteen times convection onset ($16R_c$). Penetration of the nonlinear regime is limited by computational capabilities. In a phase space, as a dynamical system, the states are characterized as: a point (S), a different point (S′), a limit cycle (P′), a torus (QP), and back to a limit cycle (P^2). The computations rapidly become unwieldly owing to spatial complexity associated with the three-dimensional domain even though the dynamics in themselves are relatively simple and well-understood. Other than the 'reverse transition' (from a quasi-periodic to a periodic motion) which is somewhat unusual (Gollub & Benson 1980 apparently observe such a transition in their experiments with pure fluids), the dynamics are not particularly interesting. On the other hand, the spatial structures are coupled to the dynamics and this coupling is crucial to the physics governing the transitions. KSS, like most authors, including Kimura, Schubert & Straus (1986), Caltagirone, Fabrie & Combarnous (1987) and Caltagirone & Fabrie (1989), who perform extensive calculations on the two-dimensional porous media case, report measures of the temporal behaviour (power spectra, time traces, frequencies) as well as plots of the spatial structures but largely ignore the connection between space and time dependence. Exceptions include Lennie *et al.* (1988), who study the relationship between spatial and temporal behaviour for two-dimensional convection (rigid horizontal and stress-free lateral boundaries) of a Boussinesq fluid with infinite Prandtl number, heated from below or within, and Graham & Steen (1991), who demonstrate a connection between various quasi-periodic dynamics and travelling wave structures for two-dimensional porous medium convection.

The transition from steady to time-periodic motion is captured in our computations using the branch-tracing approach. The three-dimensional base state, stable from slightly above convection onset, is followed as the Rayleigh number (R) increases and its linear stability characteristics are calculated simultaneously. The

base state is unstable to a small-amplitude oscillation with frequency 183.2 ± 0.5 (non-dimensional time^{-1}) at $R_p = 584 \pm 1$ (Hopf bifurcation). This corresponds to an S–P transition and is the focus of our study.

The branch-tracing technique has the advantage (relative to solving a series of initial-value problems, say) that points of bifurcation can be precisely detected, their nature identified, and the destabilizing disturbances exhibited. The latter makes a detailed understanding of the mechanism feasible. On the other hand, the disadvantage of the branch-tracing approach is the computational cost. Accurate solution of larger and larger (dense) eigenvalue–eigenvector problems (~ 1500 equations) quickly becomes prohibitive. In our calculations that yield a time-periodic instability at $R = 584$ with a frequency 183 (S–P transition), we restrict disturbances to those with symmetry or antisymmetry about the vertical diagonals. The computations of KSS are unrestricted by imposed symmetry and yield a time-periodic transition at $R = 575$ with frequency 176 (S′–P′ transition). Furthermore, spatial structures of the time-dependent states from the two calculations are nearly identical. These results suggest that the slightly asymmetric branch S′ is sufficiently like the symmetric branch S that the time-periodic instability on each branch is driven by essentially the same physics.

The results of KSS concerning the S–S′ transition are inconclusive. They find that the transition occurs somewhere between $R = 475$ and 540 depending on whether Rayleigh number is increasing or decreasing and on the size of step change in Rayleigh number. Our calculations place the S–S′ transition at $R = 495$ and taken with the KSS observations lead to a bifurcation diagram consistent with all the evidence.

The disturbance structure (the eigenvectors associated with the unstable eigenvalues) for the S–P transition is resolved to show that it is a wave travelling along a path which generally follows the circulation of the base state. A full loop of the wave has seven pairs of thermal disturbances and six pairs of vortices. The vorticity disturbances pass the thermal disturbances along the vertical leg of their journey, as was found in a study of the corresponding transition in a two-dimensional box (Steen & Aidun 1988). By a comparison with the well-understood two-dimensional problem, the influence of the third dimension is identified. The effective aspect ratio of the cubic box relative to the square box changes the ratio of time spent by a fluid packet along horizontal legs to time spent along vertical legs of trajectories. In addition there is added dissipation due to thermal diffusion in the third direction.

The relationship between two- and three-dimensional results is established through a symmetry relationship which, although nearly trivial, seems not to be widely recognized. The slippery and adiabatic sidewall boundary conditions allow every pattern in a finite container to be extended to the horizontally infinite layer by replication (a tiling process). Spatial symmetries of the flow within the repeating block (the finite container) may make a different tiling possible. The building block of the second tiling may appear to be a different finite-container flow. However, finite-container flows which generate identical infinite flows are equivalent. For example, at convection onset, the so-called cross-roll mode (the superposition of two orthogonal rolls) in a box with square planform of aspect ratio $1/\sqrt{2}$ is equivalent to a (apparently) fully three-dimensional mode in the cubic box (the [111] mode – see below). This equivalence persists into the nonlinear regime as long as the flow symmetry is preserved. Furthermore, the flows will have equivalent stabilities as long as the mode of instability shares the same symmetry as the base state. The

convection pattern whose stability we examine develops from the [111] mode and maintains its symmetry as it deforms with increasing Rayleigh number along the branch. The destabilizing oscillation preserves the same symmetry. Hence, there is an equivalent flow in a box of square planform with aspect ratio $1/\sqrt{2}$. It turns out that the mechanism of instability can be easily recognized to be related to the mechanism in two-dimensional convection, in the context of the three-dimensional box of aspect ratio $1/\sqrt{2}$.

After reviewing the governing equations and their important features, we describe the computational approach and characterize the accuracy of the solutions. After presenting the bifurcation diagram that includes the S–S′, S′–P′ and S–P transitions and briefly describing the three-dimensional steady base state, the structure of the destabilizing disturbance is presented and the evidence for a travelling wave structure is developed. A comparison of the destabilizing disturbances in two- and three-dimensional containers is drawn and finally the three-dimensional effects are discussed.

2. Formulation

Consider a closed, rectangular box, filled with a fluid-saturated porous medium. Flow within is described by Darcy's law and inertial terms are neglected (i.e. the permeability k of the medium is assumed very small). In addition, the effective thermal diffusivity of the medium is taken to be independent of velocity (i.e. the particle Péclet number is low). The horizontal top and bottom are isothermal with the bottom warmer than the top; when no motion occurs, a linear temperature gradient is present in the medium. The vertical walls are adiabatic. The buoyancy of the fluid is described by the Oberbeck–Boussinesq approximation; the variable density of the fluid is retained only in the body force term of the momentum equation. All other physical properties are constant. The box has height l and horizontal dimensions $h_1 l$ and $h_2 l$, so the aspect ratios are h_1 and h_2 (for the cube, $h_1 = h_2 = 1$). Under these conditions, the dimensionless equations governing deviations from the linear conduction state are

$$\left.\begin{aligned} \nabla\cdot\boldsymbol{v} &= 0, \\ \mathbf{0} &= -\nabla p - \boldsymbol{v} + R^{\frac{1}{2}}\theta\boldsymbol{k}, \\ \frac{\partial\theta}{\partial t} + R^{\frac{1}{2}}\boldsymbol{v}\cdot(\nabla\theta - \boldsymbol{k}) &= \nabla^2\theta, \\ \nabla\theta\cdot\boldsymbol{n} &= 0 \quad \text{on sidewalls,} \quad x = \pm\tfrac{1}{2}h_1, \quad y = \pm\tfrac{1}{2}h_2, \\ \theta &= 0 \quad \text{on top and bottom,} \quad z = 0, 1, \\ \boldsymbol{v}\cdot\boldsymbol{n} &= 0 \quad \text{on all boundaries,} \end{aligned}\right\} \tag{1}$$

where $\boldsymbol{v}$, p and θ are the velocity, pressure and temperature deviations, respectively. The Rayleigh number is $R = g\alpha\Delta T k l/\kappa_m \nu$, where α is the coefficient of thermal expansion of the fluid, g is the magnitude of the acceleration due to gravity, ΔT is the temperature difference between top and bottom, ν is the kinematic viscosity and κ_m is an effective thermal diffusivity of the fluid–solid mixture. The scales are, for velocity $R^{\frac{1}{2}}\kappa_m/l$, temperature ΔT, length l and time $l^2 H/\kappa_m$, where H is the ratio of volumetric heat capacity of the saturated medium to that of the fluid.

It is convenient to reformulate (1) as a single integro-differential equation for θ (Steen 1986); the scalar temperature field determines the velocity field uniquely. The

linearization of (1) around the null solution yields an eigenvalue problem for the stability of the conduction state; the resulting eigenfunctions are

$$\theta_i = \cos\left(\frac{p\pi}{h_1}(x+\tfrac{1}{2}h_1)\right)\cos\left(\frac{q\pi}{h_2}(y+\tfrac{1}{2}h_2)\right)\sin(r\pi z), \tag{2}$$

with corresponding eigenvalues

$$R_i = \pi^2\frac{[(p/h_1)^2+(q/h_2)^2+r^2]^2}{(p/h_1)^2+(q/h_2)^2}, \tag{3}$$

where $p = 0, 1, 2\ldots$; $q = 0, 1, 2\ldots$; $r = 1, 2, 3\ldots$; $i = [pqr]$ (Beck 1972). For a cubic box, convection onset occurs at $R_c = 4\pi^2$ with $[pqr] = [011]$ or $[101]$ (these are equivalent states, one being rotated by $\frac{1}{2}\pi$ around a vertical axis from the other). These steady states are two-dimensional rolls. The first 'three-dimensional' steady state comes into existence at $R = 4.5\pi^2$, with $[pqr] = [111]$. It becomes linearly stable at $R \approx 1.2R_c$, although the two rolls are still stable (Steen 1983). The domain of attraction of the [111] state grows as R increases. This steady state is the subject of our study. We compute how it deforms as R increases and keep track of its linear stability.

3. Computational approach

The branch of nonlinear patterns that start with the structure of the [111] mode at convection onset will be termed the 'S branch'. For fixed R we solve for a nonlinear state on the S branch by a Galerkin scheme,

$$\theta(x, y, z, t) = \sum_{i=1}^{\infty} a_i(t)\,\theta_i(x, y, z),$$

where θ_i are eigenfunctions (2) and a_i are the unknown coefficients. This choice of basis allows the coefficients in the resulting system of ODEs (formally equivalent to (1)) to be evaluated in closed form. The set of eigenfunctions used in the expansion need not be the full set. Most calculations reported here use only those that result from the nonlinear interactions of the [111] mode with itself. All such modes are either symmetric or antisymmetric under reflection across the two vertical diagonals through the centre of the box. This choice does not limit the accuracy of the steady-state calculation, though for a complete linear stability analysis, modes which break this symmetry (e.g. [101]) must be considered. The infinite system of ODEs is obtained by expanding the integro-differential equation for θ and projecting on the basis functions in the standard way,

$$\dot{a}_i = \sum_{j=1}^{\infty} L_{ij}\,a_j + \sum_{j,k=1}^{\infty} B_{ijk}\,a_j\,a_k. \tag{4}$$

Calculation of closed-form expressions for the coefficients in terms of h_1, h_2 and R is straightforward (Steen 1986). The issue of appropriate truncation of this infinite system is related to convergence and will be discussed below. Pseudo-arclength continuation (Doedel 1981) is used to compute the S branch of steady solutions from convection onset up to $R \approx 600$. The linear stability of a steady solution of (4) is calculated by finding the eigenvalues of its Jacobian evaluated at the steady state. The steady state becomes linearly unstable when an eigenvalue with positive real part appears in the spectrum.

Limitations of computation time preclude consideration of arbitrary disturbances.

Truncation order	Number of equations	R_p	f
24	650	586.7	140.1
28	1015	590.7	186.5
29	1120	580.7	180.7
30	1240	587.1	185.0
31	1360	582.4	180.6
32	1496	584.7	183.8
34	1785	583.9	183.2

Aitken–Shanks sequences of R_p:

S_0	S_1	S_2	S_3
586.7			
590.7	587.8		
580.7	584.6	584.4	
587.1	584.4	584.7	584.5
582.4	583.9	584.0	
584.7	584.1		
583.9			

TABLE 1. Values of R_p with increasing truncation order M and Aitken–Shanks sequences S_i, where i is the number of Aitken–Shanks iterations

However, it turns out that the relevant disturbances themselves retain a degree of symmetry and hence it is sufficient to consider a restricted class of modes. We distinguish three symmetry classes, each less restrictive than the previous one. First, the symmetry of the S branch is characterized by modes satisfying $p+q$, $p+r$ and $q+r$ all even (see the discussion of the three-dimensional steady base state for an alternative characterization). The second class, which includes the symmetry of the instability yielding the S′ branch, is defined by modes such that $p+r$ is odd while $q+r$ is even or vice versa. The third class includes all modes, i.e. p, q and r are arbitrary. The S–S′ bifurcation is detected by considering instabilities in the second class, and for the S–P transition only disturbances in the first class need be considered (there, the symmetry in time is broken).

We turn to the issue of truncation of the Galerkin expansion. Consider the three-dimensional space of wavenumbers $p, q, r(>0)$ of the expansion functions. Many Galerkin and pseudo-spectral studies of convection in viscous fluids and porous media use a basis corresponding to a cube in wavenumber space (McLaughin & Orszag 1982; Curry *et al.* 1984; Aidun & Steen 1986, 1987; Steen & Aidun 1988) or to a triangular pyramid (Veronis 1965; KSS). In two dimensions these regions are square and triangular, respectively. A cubic truncation contains the modes such that $p \leqslant N$, $q \leqslant N$ and $r \leqslant N$, while a triangular or diagonal one contains those satisfying $p+q+r \leqslant M$. It has been argued on qualitative grounds that the triangular truncation is superior (Veronis 1965), but no rigorous criterion exists for determining which is better. We test convergence of steady solutions (via Nusselt numbers) against truncation shape including non-square and non-triangular shapes and conclude that the triangular truncations are most efficient. All calculations reported use a triangular truncation.

The stabilities of a sequence of converged steady solutions are discussed next. All of these steady states undergo Hopf bifurcation. The critical Rayleigh numbers, R_p, and frequencies f, of the destabilizing disturbances are shown in table 1. It is apparent that R_p is converging to a value near 584. A sequence of Aitken–Shanks

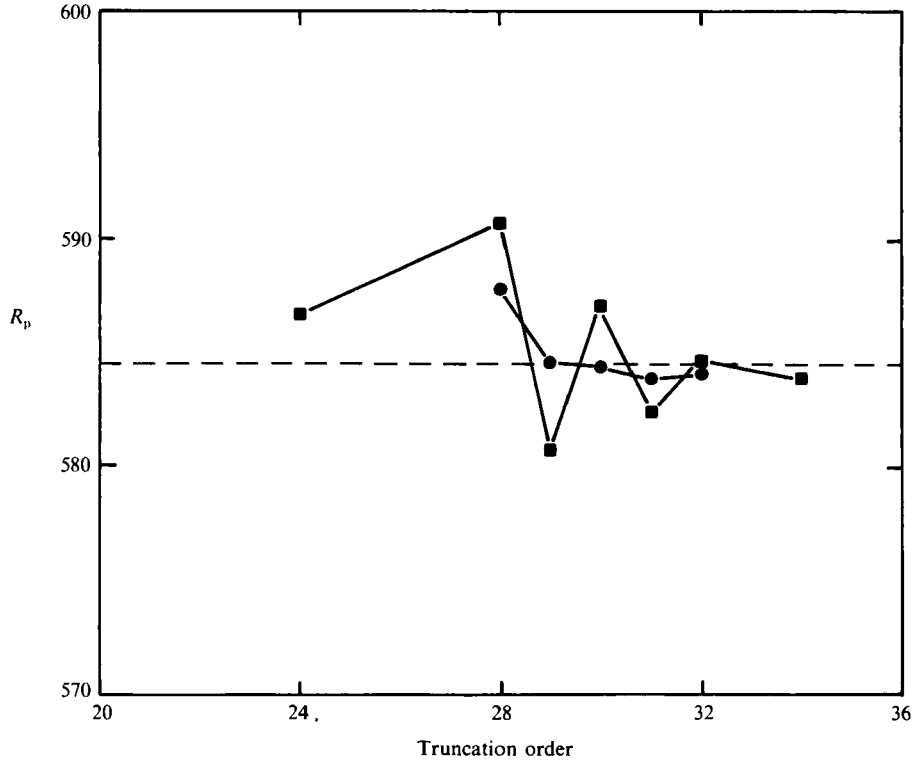

FIGURE 1. R_p *vs.* truncation order M: squares are computed values (S_0 in table 1) and circles are the first Aitken–Shanks iteration (S_1), where truncation is taken to be the middle value of the three truncation orders used in the transformation.

transformations (also shown in table 1) accelerates the convergence of the sequence, giving a final estimate of 584.5. Figure 1 shows graphically the improvement achieved by the transformations. The frequency is converging to 183 and the frequencies of the four most slowly decaying disturbances have converged to at least two significant digits. Perhaps most importantly, the structures of the destabilizing disturbances are qualitatively unchanged for all truncations with $M \geqslant 28$. The computations for the symmetry-breaking S–S′ bifurcation are performed with $M = 32$.

4. Results and discussion

4.1. S–S′ *bifurcation*

The branch of steady convection patterns S stabilizes shortly above convection onset ($R \approx 1.2R_c$) and remains stable to arbitrary infinitesimal disturbances until $R = 495$, where it destabilizes to a slightly asymmetric flow S′. The asymmetry breaks the invariance of the two vertical planes that pass through diagonals but retains a symmetry obtained by reflection across the midplane, rotation by $\frac{1}{2}\pi$ with a concommitant change of sign of θ. In view of general results from bifurcation theory (Golubitsky & Schaeffer 1985), the symmetry-breaking nature of the instability forces the bifurcation to be a pitchfork (actually a 'double pitchfork' due to symmetry). Although we are able to compute the linear stability of the symmetric

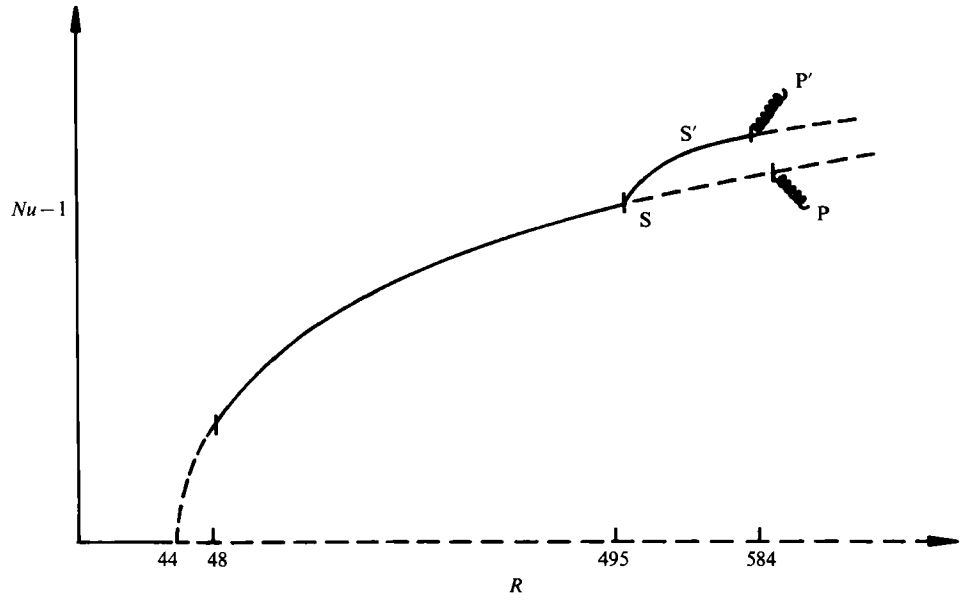

FIGURE 2. Schematic bifurcation diagram of normalized heat transfer ($Nu-1$) versus R showing S and S′ steady branches and the Hopf bifurcations P and P′ from them. Solid curves are linearly stable, broken ones unstable. The Hopf points are represented by the helical symbols.

base state to appropriate disturbances and thereby detect the branch point, we are unable to follow the S′ branch into the nonlinear regime owing to computational limitations.

Nevertheless, a consistent picture can be constructed using evidence from KSS. The computed growth rates of the infinitesimal asymmetric disturbances to the branch S for a range of R above $R = 495$ are found to be exceedingly slow. In particular, the time for the unstable asymmetric disturbance to grow tenfold is 13.6 thermal diffusion times at $R = 500$. At $R = 540$, where KSS first detect S′ on increasing R, tenfold amplification requires 0.78 diffusion times. At $R = 584$ tenfold growth requires 0.22 diffusion times. The ability to detect branch-switching via the initial-value problem approach depends on (i) the initial conditions for the calculation and (ii) the growth rate of the most unstable disturbances. If the initial condition is taken as the steady state from a lower R-value, then the amplitude of the 'infinitesimal' disturbance depends on the shape of the branch (slope, curvature, etc.) and the size of the step in R from the previous computation. In view of the relatively flat nature of the S branch (the Nusselt number Nu varies less than 3% between $R = 500$ and 540), initial conditions set in this manner will represent low-level disturbances. The shorter the step in Rayleigh number, the smaller will be the amplitudes of the initial disturbance.

All the observations of KSS concerning S–S′ branch-switching with increasing R can be explained by computation times limited to about one diffusion time. Furthermore, the S and S′ branches remain very close in phase space in this range (less than 1% difference by a Nusselt number measure) and the stability characteristics of the S branch just below $R = 495$ are similar to the instability characteristics just above $R = 495$ – i.e. very slow decay rates. This would explain the KSS observations that on decreasing R the S branch is not detected until $R = 475$. Moreover, this view is consistent with our premise that the S and S′

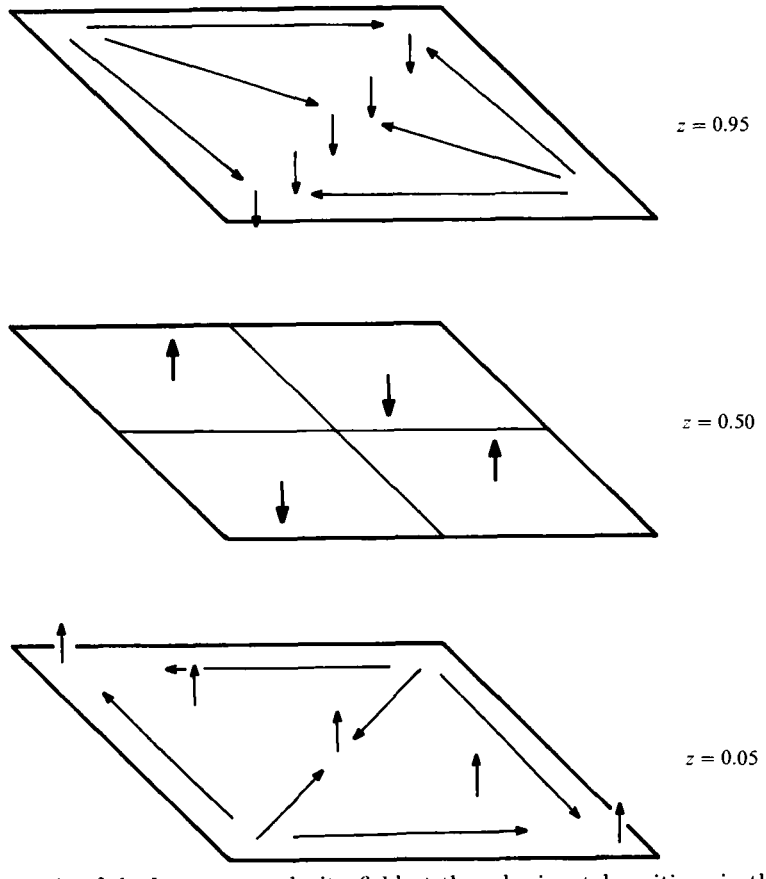

FIGURE 3. Schematic of the base-state velocity field at three horizontal positions in the cube.

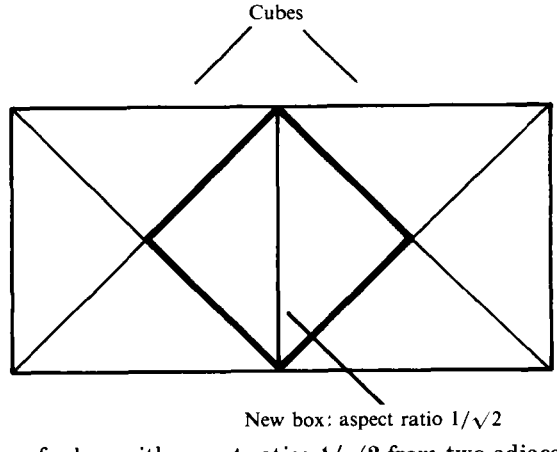

FIGURE 4. Construction of a box with aspect ratios $1/\sqrt{2}$ from two adjacent cubes, viewed from the top. Because of symmetry, this box or the cube offer alternative basic cells for a periodic tiling.

branches are sufficiently similar to share the same mechanism of instability to time-periodic disturbances. In summary, evidence suggests a bifurcation diagram near the S–P and S′–P′ transitions as shown in figure 2. Henceforth we discuss only the S and P states.

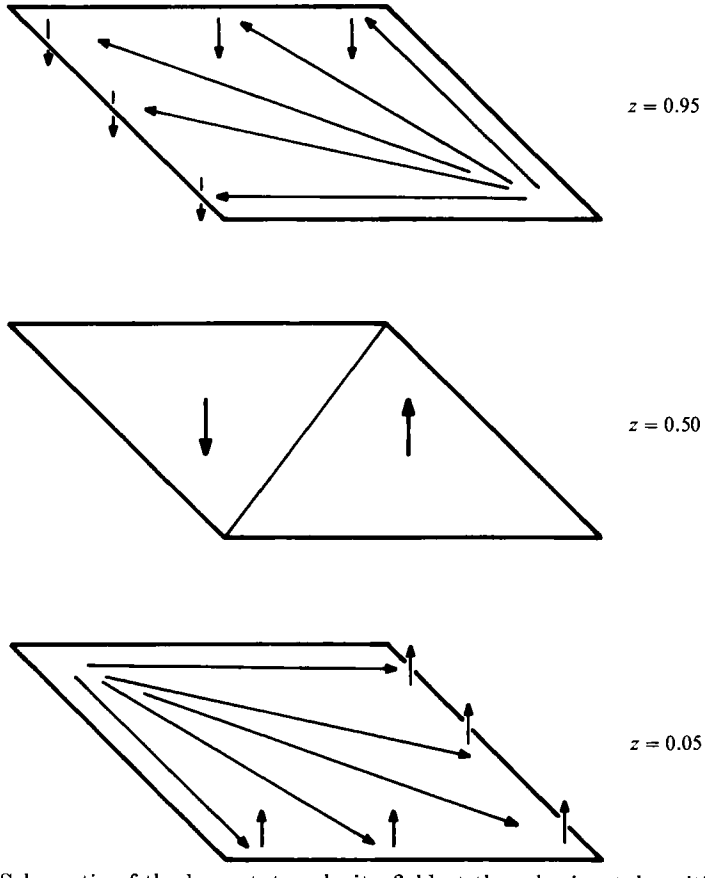

FIGURE 5. Schematic of the base-state velocity field at three horizontal positions in the $1/\sqrt{2}$ box.

4.2. *The three-dimensional steady base state* (*S*)

Figure 3 shows the general nature of the base state: cold fluid in two of the bottom corners of the box flows across the bottom toward the diagonal, picking up heat; the flow near this diagonal is a reverse 'stagnation line' flow; the now warm fluid accelerates up from the diagonal and splits into two upward-moving lobes at the horizontal midplane of the box; the fluid reaches the top of the box to again flow from corners to diagonal, but now releasing heat to the cool top before accelerating back downward to split into two downward-moving lobes. In the top corners, to which hot fluid is convected, and the bottom corners, to which cold fluid moves, steep, unstably stratified temperature gradients develop as R increases. Figure 3 shows clearly that the velocity (and temperature) fields are mirror symmetric across the vertical diagonal planes through the centre of the box, so that in essence, these planes are no-flux boundaries. In addition, the velocity is invariant, and the sign of the temperature changed, under reflection through the horizontal midplane followed by rotation by $\frac{1}{2}\pi$ around a vertical axis through the centre of the box. If, for the moment, the origin is placed at the centre of the cube, these symmetries can be expressed as

$$\theta(x,y,z) = \theta(y,x,z),$$
$$\theta(x,y,z) = \theta(-y,-x,z),$$
$$\theta(x,y,z) = -\theta(y,x,-z).$$

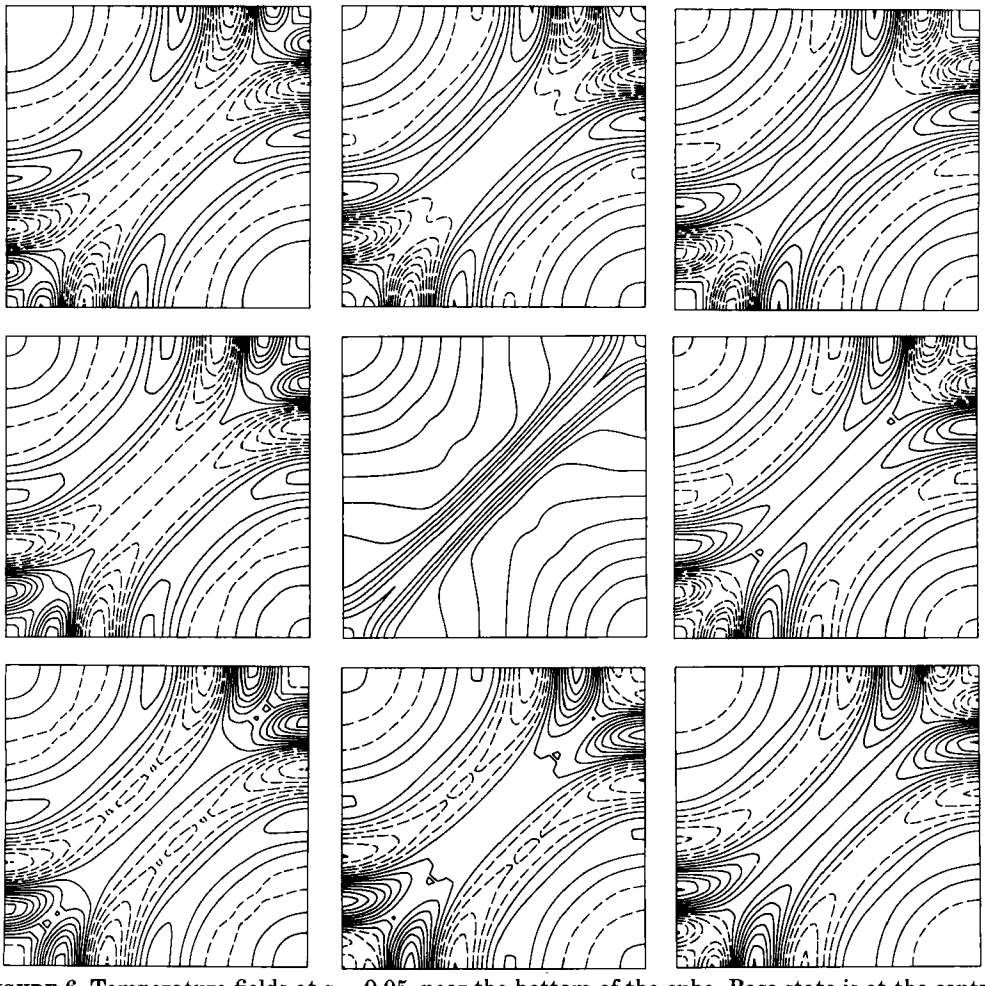

FIGURE 6. Temperature fields at $z = 0.05$, near the bottom of the cube. Base state is at the centre, surrounded in clockwise progression by the disturbance at intervals of $\frac{1}{8}$ period. Time increases clockwise; $t = 0$ is at the upper left. Solid lines represent positive disturbance, and dashed ones, negative.

Owing to these symmetries, each of the four triangular prisms bounded by the walls and vertical diagonals are invariant and identical to within a reflection. We shall take advantage of this invariance to clarify the nature of the steady state, and later, the disturbance.

Consider two adjacent cubes in which convection is occurring, as shown in figure 4. Because of the symmetries, the rectangular box between diagonals of the original cubes is invariant, and the flow in it satisfies the same boundary conditions as imposed on the walls of the cube. This new box can be treated just as the cube was, but it has aspect ratios $h_1 = h_2 = 1/\sqrt{2}$. Convection onset in a box of this geometry occurs via simultaneous bifurcation of the [011] and [101] modes (two-dimensional rolls) at $R_c = 4.5\pi^2$ (Beck 1972). This is the same critical Rayleigh number at which the [111] mode appears in the cube, and through a coordinate transformation the [111] mode in the cube is identical to an equal superposition of the [011] and [101] modes in the new box. Thus the flow in the new box is simply the nonlinear evolution of two orthogonal rolls, a cross-roll. The base-state velocity is shown schematically

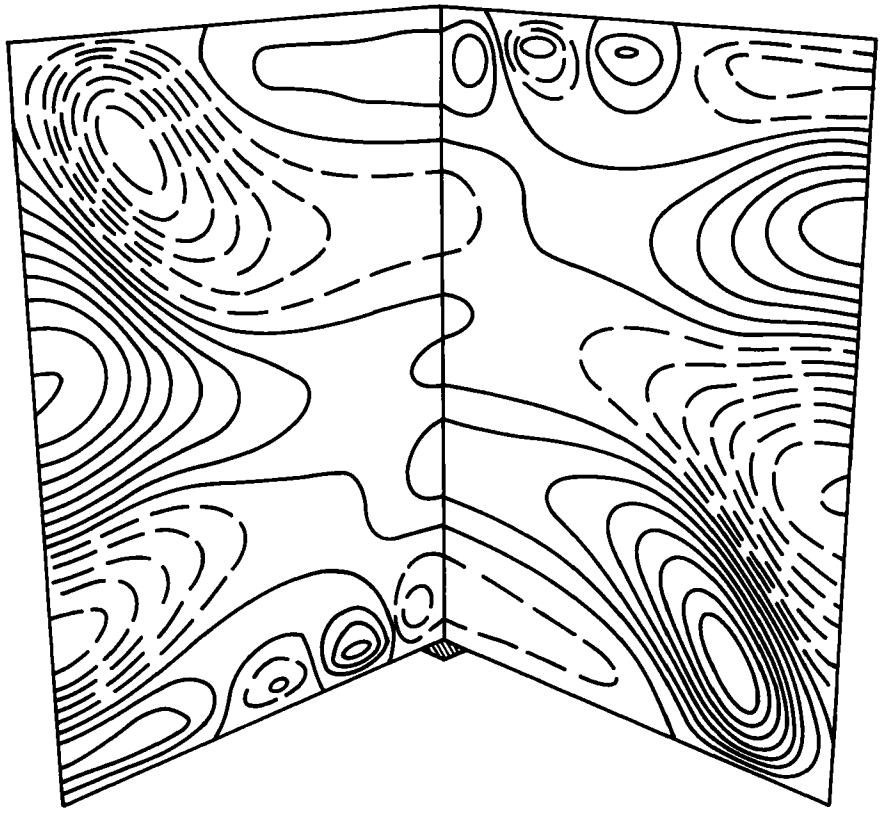

FIGURE 7. Disturbance temperature field on vertical diagonals through the centre of the cube at $t = 0$.

in figure 5. The flow is symmetric across the vertical diagonal that is the common sidewall of the two original cubes used to form the new box. If the two rolls did not interact, the two-dimensional evolution of one of them would represent the behaviour of the entire flow. Thus, the flow in the cube would be the superposition of two orthogonal, but otherwise identical, two-dimensional structures. Of course, the rolls do interact, yielding the three-dimensional effects that will be discussed in §4.5.

4.3. *Structure of the three-dimensional disturbance* (S–P)

We present here the results from an $M = 30$ triangular truncation, for which $R_p = 587.1$ and $f = 185.0$. The centre plot in figure 6 shows the isotherms of the steady state at a horizontal surface near the bottom of the box in the thermal layer where temperature gradients are steep ($z = 0.05$). In this and all base-state plots, we add the linear temperature profile. Disturbance isotherms are shown in clockwise progression around the box at intervals of $\frac{1}{8}$ of an oscillation period. Solid lines represent positive disturbance θ, and dashed ones, negative. A wavy structure is evident in the disturbance. The alternating cold and hot regions are propagating from the two corners where gradients are steep toward a diagonal, in the same manner as the base flow (cf. figure 3). We can also see, in this plane at least, that the disturbance preserves the spatial symmetries of the base state. It turns out that these symmetries are preserved throughout the box. Figure 7 shows disturbance isotherms on the vertical diagonals connecting opposite corners of the cube. It is clear that

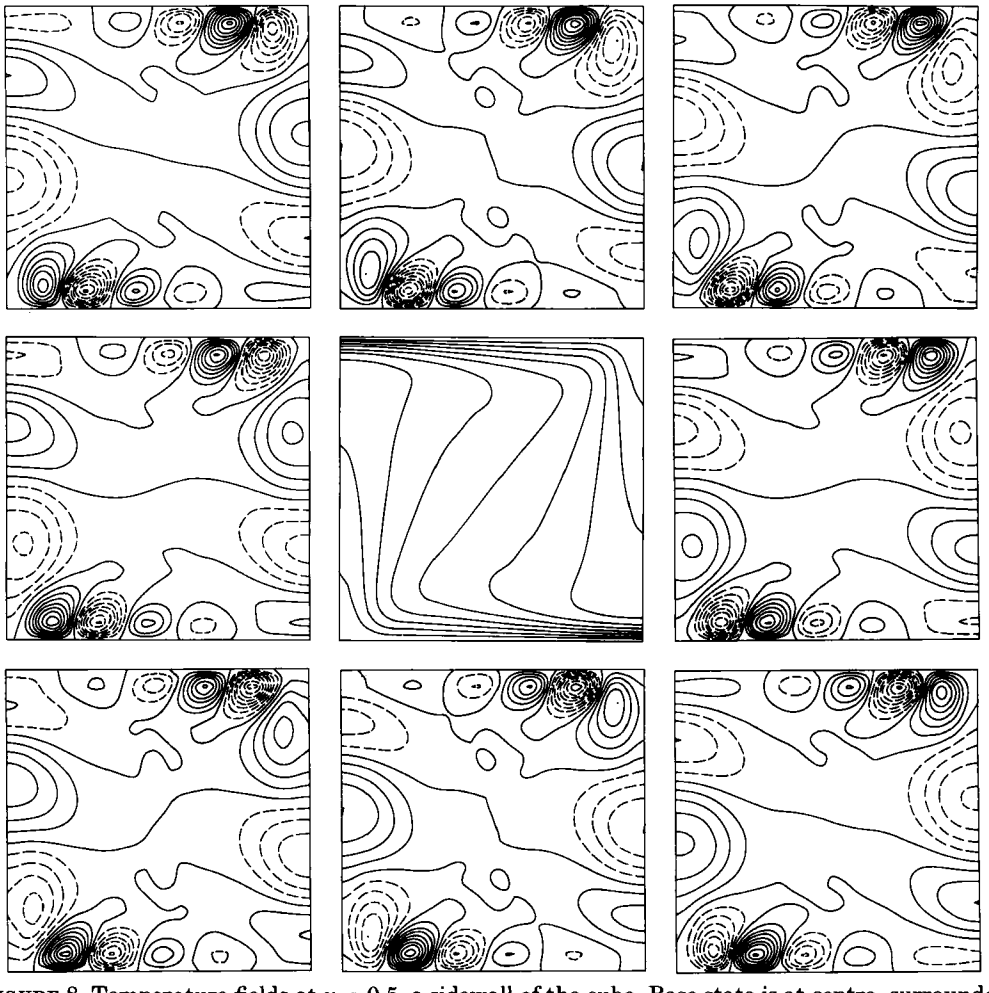

FIGURE 8. Temperature fields at $y = 0.5$, a sidewall of the cube. Base state is at centre, surrounded by the disturbance. Same sequence as figure 6. The base flow on this wall is clockwise.

seven pairs of thermal blobs are present. A disturbance starting in the lower right corner moves across the bottom of the box in roughly two periods, lifts up from the bottom at the diagonal, splitting as it moves through the centre of the box in another 1.5 periods to the top corners, where the process repeats, and the blob returns to the bottom. The entire process takes seven periods. Figure 8 shows the thermal base state (centre) and disturbance on a sidewall, $y = 0.5$, where the disturbance is strongest. Figure 9 shows the vorticity disturbance corresponding to the isotherms of figure 8. The vorticity at the walls is perpendicular to the walls because of the boundary conditions, so it can be regarded as a scalar. There are six pairs of vorticity blobs, and one of them slips past two thermal blobs on the adiabatic sidewall. A vorticity blob takes 2 periods to traverse the bottom, but then only 1 instead of 1.5 to reach the top, so each vorticity blob traverses the box in 6 periods.

The nature of the disturbance is clarified by examining the energy equation, linearized about the steady state,

$$\frac{\partial \hat{\theta}}{\partial t} + R^{\frac{1}{2}} \bar{\boldsymbol{v}} \cdot \boldsymbol{\nabla} \hat{\theta} = \nabla^2 \hat{\theta} - R^{\frac{1}{2}} \hat{\boldsymbol{v}} \cdot (\boldsymbol{\nabla} \bar{\theta} - \boldsymbol{k}), \tag{5}$$

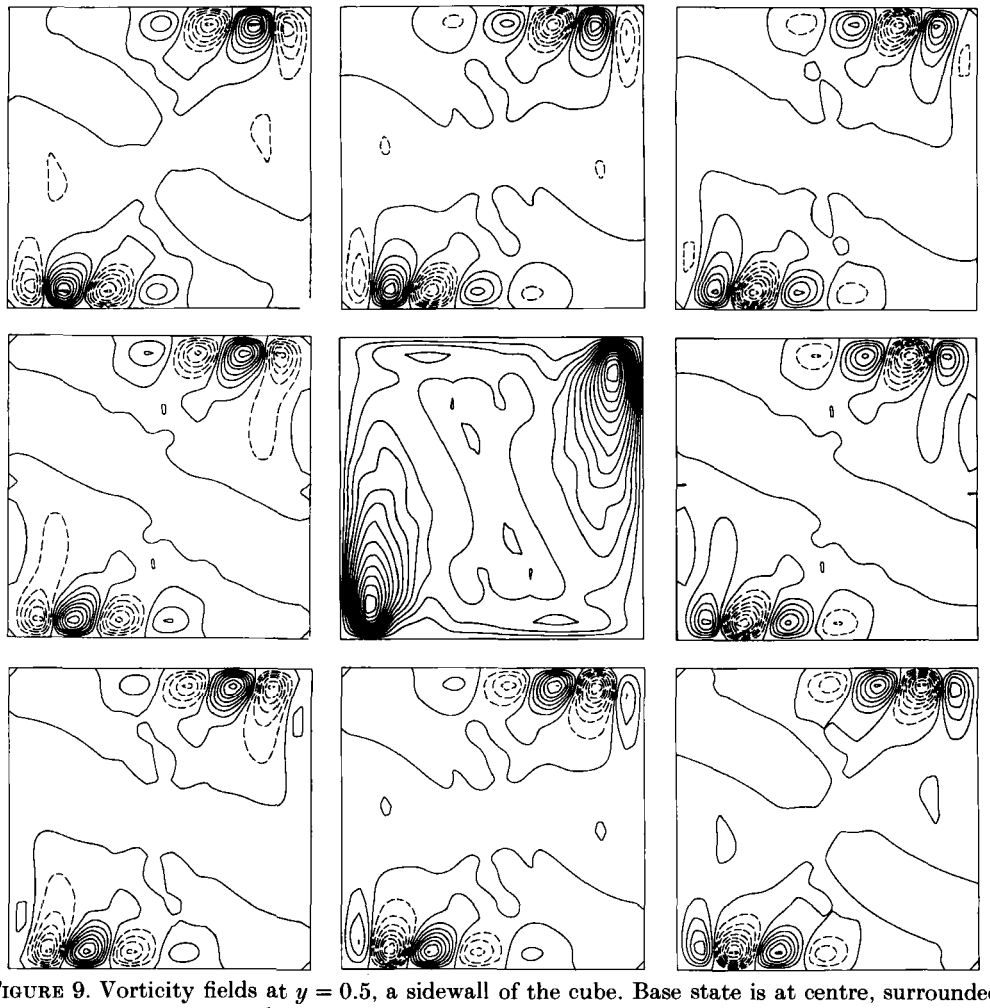

FIGURE 9. Vorticity fields at $y = 0.5$, a sidewall of the cube. Base state is at centre, surrounded by disturbance. Same sequence as figure 6.

where bars and hats denote base-state and disturbance quantities, respectively. This equation can be rewritten as

$$\frac{\partial \hat{\theta}}{\partial t} + R^{\frac{1}{2}} \bar{\boldsymbol{v}} \cdot \boldsymbol{\nabla} \hat{\theta} = \boldsymbol{\Phi} = \nabla^2 \hat{\theta} - R^{\frac{1}{2}} \hat{\boldsymbol{v}} \cdot (\boldsymbol{\nabla} \bar{\theta} - \boldsymbol{k}), \tag{6}$$

where $\boldsymbol{\Phi}$ represents the coupling between the left- and right-hand sides. One way to measure $\boldsymbol{\Phi}$, the coupling function, is to multiply (6) by $\hat{\theta}$ and integrate over the volume of the cube. This yields

$$\frac{\mathrm{d}}{\mathrm{d}t} \langle \tfrac{1}{2} \hat{\theta}^2 \rangle = \langle \hat{\theta} \boldsymbol{\Phi} \rangle = \langle \hat{\theta} \nabla^2 \hat{\theta} \rangle - R^{\frac{1}{2}} \langle \hat{\theta} \hat{\boldsymbol{v}} \cdot \boldsymbol{\nabla} \bar{\theta} \rangle + R^{\frac{1}{2}} \langle \hat{\theta} \hat{\boldsymbol{v}} \cdot \boldsymbol{k} \rangle, \tag{7}$$

where $\langle \cdot \rangle$ represents integration over the volume. Evaluating these terms at the solution for oscillation onset yields $\langle \hat{\theta} \boldsymbol{\Phi} \rangle$, a measure of the coupling. If $\boldsymbol{\Phi} \equiv 0$ the left- and right-hand sides decouple.

This decomposition by decoupling was first discussed in the context of two-dimensional convection, where $\langle \hat{\theta} \boldsymbol{\Phi} \rangle$ is less than 1% of $\langle \hat{\theta} \nabla^2 \hat{\theta} \rangle$, the largest term on

the right-hand side (Steen & Aidun 1988). We summarize that discussion. Consider first the left-hand side, where $\hat{\theta}$ is viewed as unknown and $\bar{\boldsymbol{v}}$ as prescribed:

$$\frac{\partial \hat{\theta}}{\partial t} + R^{\frac{1}{2}} \bar{\boldsymbol{v}} \cdot \boldsymbol{\nabla} \hat{\theta} = \Phi \approx 0. \tag{8}$$

This equation for convection of disturbance temperature by base-state velocity is a first-order wave equation. It suggests that the thermal disturbance is convected with the steady flow as a travelling wave with wave speed $R^{\frac{1}{2}}\bar{\boldsymbol{v}}$. This equation governs 'propagation'. The presence of the factor $R^{\frac{1}{2}}$ is due to the different scalings of time and velocity.

The right-hand side of (6) in the limit of decoupling can be rewritten

$$\nabla^2 \hat{\theta} = R^{\frac{1}{2}} \hat{\boldsymbol{v}} \cdot (\boldsymbol{\nabla} \bar{\theta} - \boldsymbol{k}). \tag{9}$$

This equation represents a balance between diffusion of disturbance energy and convection of base-state energy via disturbance velocity and is elliptic in nature. Note that the momentum equation governing disturbances can be solved for and substituted in (9) to eliminate $\hat{\boldsymbol{v}}$ in favour of $\hat{\theta}$ and the disturbance pressure field $\hat{p}$,

$$\nabla^2 \hat{\theta} = (R\hat{\theta}\boldsymbol{k} - R^{\frac{1}{2}} \boldsymbol{\nabla} \hat{p}) \cdot (\boldsymbol{\nabla} \bar{\theta} - \boldsymbol{k}). \tag{10}$$

Note, furthermore, that $\hat{p}$ is a functional of the temperature field $\hat{\theta}$ so that (10) is effectively an equation for the unknown scalar temperature field $\hat{\theta}$ with coefficients determined by the base-state field $\bar{\theta}$. Equation (10) can then be viewed as determining the 'structure' of the disturbance, given the base state. Once the structure is determined, it may be used as an initial condition in (8), which then determines its propagation.

The success of this approach was demonstrated in two dimensions (Steen & Aidun 1988). There, the domain for (8) and (9) was assumed to be a characteristic loop determined by the base flow. A transplantation of (8) and (9) onto the one-dimensional loop domain leads to a modified Mathieu–Hill equation governing the disturbance structure. Solutions of this eigenvalue problem fit on the loop first with increasing Rayleigh number at $R = 390 \pm 10$ and only with five pairs of thermal disturbances. This matches the exact results closely (see below). In other words, the structure equation predicts both the Rayleigh number at oscillation onset and the disturbance wavenumber.

The primary balance represented by (9) or (10) is between convection of the base-state thermal field by buoyancy-generated disturbance velocity and thermal diffusion of disturbances. However, disturbance velocities generated by pressure gradients also influence wavenumber selection and explain why, for example, travelling waves with five pairs of thermal blobs destabilize before those with three pairs for the square box, while the reverse occurs for shallower boxes (aspect ratio greater than about 2.5, Graham & Steen 1991). In summary, not only must thermal gradients be sufficiently large to destabilize the thermal boundary layers of the base state, but the disturbance velocity must be of phase such that the disturbances 'fit' on the loop. An alternative view of similar structures that arise in pure fluid Boussinesq convection, heated from below or within, is offered by Lennie *et al.* (1988). In that study, as in the present one, the initial Hopf bifurcations arise owing to convected thermal boundary-layer instabilities. The mechanisms for further transitions differ, however, because the boundary-layer fluctuations develop differently in the internally heated and heated-from-below cases. In the internal heating case, period-doubling or quasi-periodic behaviour occurs because of plumes which burst out of the

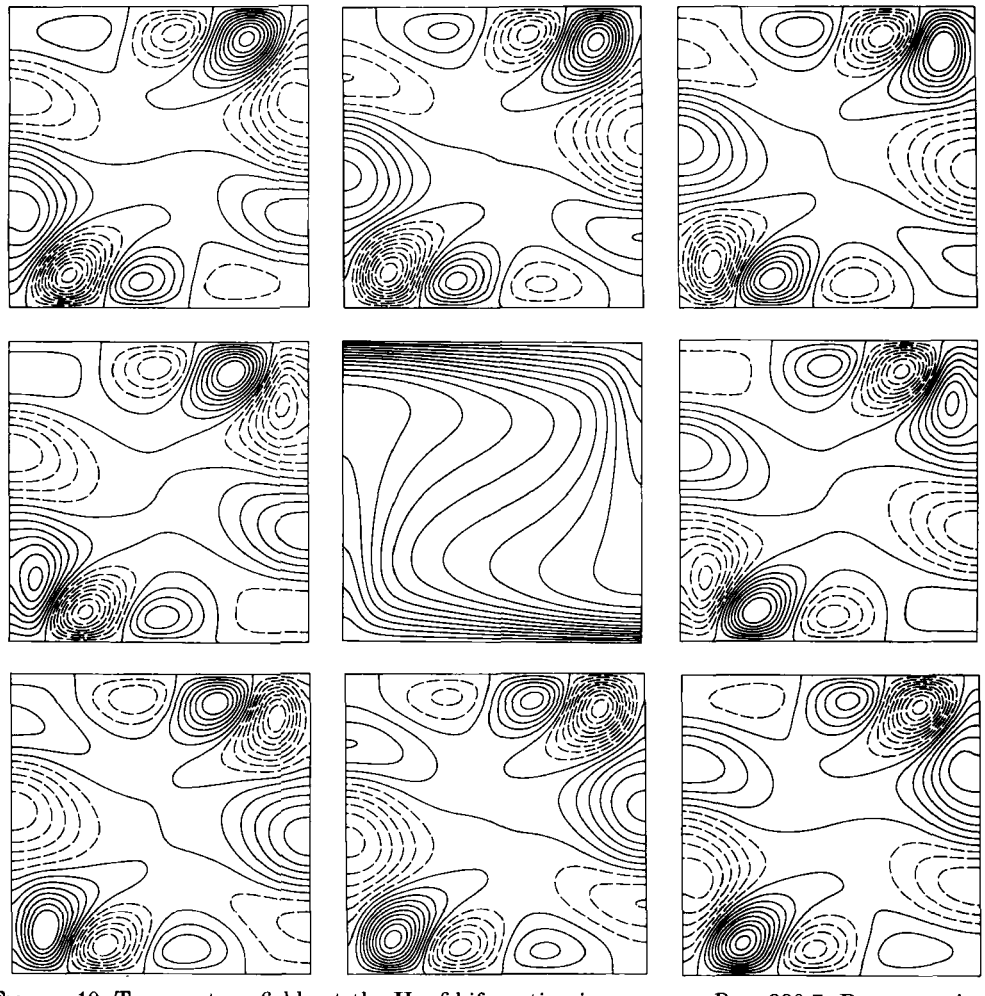

FIGURE 10. Temperature fields at the Hopf bifurcation in a square, $R_p = 390.7$. Base state is at centre, surrounded by disturbance. Same sequence as figure 6.

boundary layer. In the two-dimensional saturated porous medium heated from below, quasi-periodic behaviour and reverse transitions occur owing to interactions between Hopf bifurcations corresponding to boundary-layer instabilities of differing wavenumbers (Graham & Steen 1991).

After developing the similarities between the two- and three-dimensional disturbances in the next section for comparison purposes, we contrast them in the last section in order to resolve the three-dimensional effects.

4.4. *Comparison of the two- and three-dimensional disturbances*

The transition to two-dimensional oscillatory convection in a square domain occurs at $R_p = 390.7$ with frequency $f = 82.8$ (Aidun & Steen 1986). The temperature disturbance consists of five pairs of blobs convected around the box by the base-state velocity. This structure is shown in figure 10. Comparison with figure 8 shows the obvious similarity between the two- and three-dimensional structures. The apparent differences are the much stronger boundary-layer temperature gradient of the base state and the higher wavenumber of the disturbance in the three-dimensional case. In the square, there are four pairs of vorticity blobs, while in the cube, there are six.

In both cases, vorticity disturbances pass thermal ones as they travel vertically. Furthermore, for the cube the coupling constant $\langle\hat{\theta}\Phi\rangle$ is also relatively small, although not as small as in the case of the square. This suggests that the decoupling of structure and propagation also holds for the cube, and that the essential mechanism for the oscillatory transition is common to both the two- and three-dimensional cases. This conclusion is not surprising given the fact that the three-dimensional flow is simply the nonlinear evolution of two interacting two-dimensional rolls, as discussed above.

In both two and three dimensions, the sequence of further transitions is marked by periodic regimes separated in Rayleigh number by regimes of quasi-periodic behaviour and hysteresis (Kimura *et al.* 1986; Caltagirone & Fabrie 1989; KSS). In two dimensions this sequence is due to interactions between Hopf bifurcations, as mentioned above. Computations show that there is a similar set of Hopf bifurcations in three dimensions, only the first of which is discussed here. These computations and the demonstrated similarity between the Hopf bifurcations in two and three dimensions suggest that the two-dimensional mechanism for further transitions may also apply to the three-dimensional transitions.

4.5. *Three-dimensional effects*

The strong similarities between the disturbances in the square and the cube suggest that two-dimensional effects are important in determining the critical Rayleigh number and disturbance structure in the cube. This is indeed so. Recall that the [111] mode in the cube is equivalent to the superposition of the [101] and [011] rolls in a box with $h_1 = h_2 = 1/\sqrt{2}$. In a box of this geometry, the roll undergoes a Hopf bifurcation at $R_p = 536.7$. The frequency is 123.2 and the wavenumber of the thermal disturbance is five. If only two-dimensional effects were present, these would be the characteristics of the Hopf bifurcation of the [111] state in the cube. Hence three-dimensional effects must account for the further increase in R_p from 537 to 584, and the increase in wavenumber from five to seven. Of course the two orthogonal rolls interact to produce three-dimensional modes. For example, their first-order interaction yields the [112] mode (in the new box). It is known that near convection onset, this mode decreases the heat transfer from that of either of the orthogonal rolls (Zebib & Kassoy 1978).

The stabilization of the flow by three-dimensional effects is related to the more rapid decay due to diffusion of a heat source in three dimensions relative to that in two dimensions. It can be understood through equation (10), which is observed to hold approximately at oscillation onset for the cubic box as well as for the square domain. Ignoring effects of disturbance pressure for the time being, this is an eigenvalue problem with 'eigenvalue' $R(\mathrm{d}\bar{\theta}/\mathrm{d}z - 1)$ which characterizes the energy transfer from the base state ($-R$ due to conduction and $R(\mathrm{d}\bar{\theta}/\mathrm{d}z)$ due to steady convection). In order to balance the increase in $\nabla^2\hat{\theta}$ in three dimensions, the energy transfer to disturbances must increase, which can occur through an increase in R or $\mathrm{d}\bar{\theta}/\mathrm{d}z$ or both. Both increases are observed. The increase in wavenumber is primarily related to the more rapid conductive decay in three dimensions, but may also be influenced by the pressure field, probably in much the same way as occurs in two dimensions.

A quantitative account of the influence of three-dimensional effects is possible and would follow the line developed in the two-dimensional case (Steen & Aidun 1988). However, since these effects are relatively less important than two-dimensional geometric effects, they will not be pursued here.

We summarize by discussing the three-dimensional distribution of disturbance strength relative to the two-dimensional case. The disturbance is strongest on the sidewalls of the cube, as can be seen clearly in figure 6. We can also see from this figure that the disturbance wavefronts are nearly circular arcs, indicating that the wave speed does not vary significantly with position at the bottom of the box, so a disturbance propagating along a sidewall spends longer in the thermal layers than does a disturbance propagating in the interior of the cube. Therefore, the disturbance is strongest on the sidewalls because it is there that a disturbance is exposed longest to the destabilizing temperature gradient. One may think of the sidewalls as having an effective aspect ratio of unity, and the diagonals, where the disturbance is weakest, as having effective aspect ratio $1/\sqrt{2}$. At convection onset and at oscillation onset in two dimensions it is known that the critical Rayleigh number and thermal gradient strength increase as aspect ratio decreases from unity because of the relative time disturbances spend moving horizontally, accumulating energy, and moving vertically, dissipating it. The distribution of disturbance strength in the cube is another manifestation of this effect. The disturbance develops primarily on the sidewalls, with three-dimensional influences extending its structure throughout the cube.

5. Conclusions

Stable steady three-dimensional convection in a cube possesses spatial symmetries as well as the symmetry of time-invariance. It first suffers a spatial symmetry-breaking instability followed by a breaking of the temporal symmetry. The nature of the bifurcation diagram in the neighbourhood of the S–P bifurcation is clarified.

Transition to time-dependent motion in the cube occurs as a Hopf bifurcation to a travelling wave structure with seven pairs of thermal blobs and six pairs of vortices. The wave travels on a path (loop) determined by the average base flow along which disturbances are sustained by self-induced buoyancy-driven convection. Evidence suggests that the number of disturbances is determined by how many can fit on a closed path for given driving force, just as in the two-dimensional case. Indeed, a coordinate transformation maps the flow into a box of aspect ratio $1/\sqrt{2}$. This geometric effect accounts for 76% of the increase in R_p over that in the two-dimensional square domain. The remaining 24% of the stabilization is attributable to greater thermal diffusion in directions orthogonal to the direction of propagation of the wave.

This work was partially supported by AFOSR and NSF DMS-8915672 and partially supported by the US Army Research Office through the Mathematical Sciences Institute of Cornell University. Numerical simulations reported here were performed at the Cornell National Supercomputer Facility, a resource of the Cornell Theory Center, which is funded in part by the National Science Foundation, New York State, the IBM Corporation and members of the Center's Corporate Research Institute.

REFERENCES

Aidun, C. K. & Steen, P. H. 1986 Transition to unsteady convective heat transfer in a fluid-saturated porous medium. *AIAA/ASME 4th Joint Thermophysics and Heat Transfer Conf., AIAA Paper* 86–1264.

AIDUN, C. K. & STEEN, P. H. 1987 Transition to oscillatory convective heat transfer in a fluid-saturated porous medium. *J. Thermophys. Heat Transfer* **1**, 268–273.

BECK, J. L. 1972 Convection in a box of porous material saturated with fluid. *Phys. Fluids* **15**, 1377–1383.

CALTAGIRONE, J.-P. & FABRIE, P. 1989 Natural convection in a porous medium at high Rayleigh numbers Part I – Darcy's model. *Eur. J. Mech.* B**8**, 207–227.

CALTAGIRONE, J.-P., FABRIE, P. & COMBARNOUS, M. 1987 De la convection naturelle oscillante en milieu poreux an chaos temporel? *C. R. Acad. Sci. Paris* **305** (II), 549–553.

CURRY, J. H., HERRING, J. R., LONCARIC, J. & ORSZAG, S. A. 1984 Order and disorder in two- and three-dimensional Bénard convection. *J. Fluid Mech.* **147**, 1–38.

DOEDEL, E. J. 1981 AUTO: a program for the automatic bifurcation analysis of autonomous systems. *Congressus Numerantum* **30**, 265–284. (Also *Proc. 10th Manitoba Conf. on Numerical Mathematics and Computation, University of Manitoba, Winnepeg, Canada, 1980*).

FABRIE, P. 1986 Solutions fortes et comportement asymptotique pour un modèle de convection naturelle en milieu poreux. *Acta Applicandae Mathematicae* **7**, 49–77.

GOLLUB, J. P. & BENSON, S. V. 1980 Many routes to turbulent convection. *J. Fluid Mech.* **100**, 447–470.

GOLUBITSKY, M. G. & SCHAEFFER, D. G. 1985 *Singularities and Groups in Bifurcation Theory*, vol. 1. Springer.

GRAHAM, M. D. & STEEN, P. H. 1991 Strongly interacting traveling waves and quasiperiodic dynamics in porous medium convection. *Physica* D (submitted).

HORNE, R. N. 1979 Three-dimensional natural convection in a confined porous medium heated from below. *J. Fluid Mech.* **92**, 751–766.

KIMURA, S., SCHUBERT, G. & STRAUS, J. M. 1986 Route to chaos in porous-medium thermal convection. *J. Fluid Mech.* **207**, 153–189.

KIMURA, S., SCHUBERT, G. & STRAUS, J. M. 1989 Time-dependent convection in a fluid-saturated porous cube heated from below. *J. Fluid Mech.* **207**, 153–189 (referred to herein as KSS).

LENNIE, T. B., MCKENZIE, D. P., MOORE, D. R. & WEISS, N. O. 1988 The breakdown of steady convection. *J. Fluid Mech.* **188**, 47–85.

MCLAUGHLIN, J. B. & ORSZAG, S. A. 1982 Transition from periodic to chaotic thermal convection. *J. Fluid Mech.* **122**, 123–142.

STAMPS, D. W., ARPACI, V. S. & CLARK, J. A. 1990 Unsteady three-dimensional natural convection in a fluid saturated porous medium. *J. Fluid Mech.* **213**, 377–396.

STEEN, P. H. 1983 Pattern selection for finite-amplitude convection states in a box of porous media. *J. Fluid Mech.* **136**, 219–241.

STEEN, P. H. 1986 Container geometry and the transition to unsteady Bénard convection in porous media. *Phys. Fluids* **29**, 925–933.

STEEN, P. H. & AIDUN, C. K. 1988 Time-periodic convection in porous media: transition mechanism. *J. Fluid Mech.* **196**, 263–290.

TITI, E. S. 1991 Gevrey class regularity and long time approximations for 3-D convection in porous media (in preparation).

VERONIS, G. 1965 Large-amplitude Bénard convection. *J. Fluid Mech.* **26**, 49–68.

ZEBIB, A. & KASSOY, D. R. 1978 Three-dimensional natural convection motion in a confined porous medium. *Phys. Fluids* **21**, 1–3.